

Mapping local orientation of aligned fibrous scatterers for cancerous tissues using backscattering Mueller matrix imaging

Honghui He
Minghao Sun
Nan Zeng
E. Du
Shaoxiong Liu
Yihong Guo
Jian Wu
Yonghong He
Hui Ma

Mapping local orientation of aligned fibrous scatterers for cancerous tissues using backscattering Mueller matrix imaging

Honghui He,^a Minghao Sun,^{a,b} Nan Zeng,^a E. Du,^{a,b} Shaoxiong Liu,^c Yihong Guo,^{a,b} Jian Wu,^a
Yonghong He,^a and Hui Ma^{a,b,*}

^aTsinghua University, Institute of Optical Imaging and Sensing, Graduate School at Shenzhen, Shenzhen Key Laboratory for Minimal Invasive Medical Technologies, Shenzhen 518055, China

^bTsinghua University, Department of Physics, Beijing 100084, China

^cHuazhong University of Science and Technology Union Shenzhen Hospital, Shenzhen Sixth People's Hospital (Nanshan Hospital), Shenzhen 518052, China

Abstract. Polarization measurements are sensitive to the microstructure of tissues and can be used to detect pathological changes. Many tissues contain anisotropic fibrous structures. We obtain the local orientation of aligned fibrous scatterers using different groups of the backscattering Mueller matrix elements. Experiments on concentrically well-aligned silk fibers and unstained human papillary thyroid carcinoma tissues show that the m_{22} , m_{33} , m_{23} , and m_{32} elements have better contrast but higher degeneracy for the extraction of orientation angles. The m_{12} and m_{13} elements show lower contrast, but allow us to determine the orientation angle for the fibrous scatterers along all directions. Moreover, Monte Carlo simulations based on the sphere-cylinder scattering model indicate that the oblique incidence of the illumination beam introduces some errors in the orientation angles obtained by both methods. Mapping the local orientation of anisotropic tissues may not only provide information on pathological changes, but can also give new leads to reduce the orientation dependence of polarization measurements. © The Authors. Published by SPIE under a Creative Commons Attribution 3.0 Unported License. Distribution or reproduction of this work in whole or in part requires full attribution of the original publication, including its DOI. [DOI: [10.1117/1.JBO.19.10.106007](https://doi.org/10.1117/1.JBO.19.10.106007)]

Key words: polarization; Mueller matrix; Monte Carlo simulation; orientation angle; cancerous tissues.

Paper 140509PR received Aug. 7, 2014; revised manuscript received Sep. 22, 2014; accepted for publication Sep. 25, 2014; published online Oct. 15, 2014.

1 Introduction

Polarization imaging techniques have shown potentials in medical diagnosis.¹ For instance, degree of polarization (DOP) and difference polarization imaging methods have been used for the detection of cancerous skin tissues.^{2,3} Mueller matrix contains rich information on the scattering media,^{4,5} therefore is also used to obtain the microstructural information on superficial biological tissues, such as the sizes and shapes of cells and their intracellular structures.^{6–8} Because the polarization states of the scattered light are more sensitive to the subwavelength “small” scatterers,^{8,9} polarization measurements are capable of detecting the cancer-induced crowded organelles in isotropic tissue samples.¹⁰ The experimental results on human colon, cervix, and skin cancerous tissues indicated that the backscattering Mueller matrix may serve as a noninvasive tool for cancer diagnosis.^{11–13} Many tissues contain aligned anisotropic fibrous microstructures, such as the collagen and elastin fibers in epithelial tissues, muscle fibers in cardiac and skeletal muscle tissues. Changes of these fibrous structures can also be characterized by polarization sensitive measurements.¹⁴ However, many studies have shown that the parameters related to linear polarization measurements such as the DOP and the majority of Mueller matrix elements may change significantly when the fibrous samples take different orientations.^{15,16} Such “sample orientation dependence” for polarization sensitive measurements

can seriously affect any efforts to quantitatively characterize the microstructure of the anisotropic samples.¹⁷

In a previous study, we have shown that the sample orientation dependence can be effectively reduced using a group of new polarization parameters obtained from Mueller matrix transformation (MMT) methods.^{9,17} These polarization parameters, A and b , are functions of the Mueller matrix elements but are not sensitive to the orientation of the fibrous structure. The MMT method also allows us to extract information on the orientations of fibers.⁹ Accurately mapping the orientations of the aligned fibers is not only important for characterizing the microstructure of the anisotropic sample, but also necessary for calculating, and later removing, the sample orientation dependence of the Mueller matrix elements.

In this paper, we propose a quantitative technique to determine the orientation of aligned fibrous scatterers. By conducting both the experiments on silk phantom and Monte Carlo (MC) simulations based on the sphere-cylinder scattering model (SCSM),¹⁸ we calculate the orientation axis parameters from different groups of Mueller matrix elements. We also compare the effective ranges and signal-to-noise ratios of the parameters, and testify their possible applications for biological tissues. The experimental results of unstained human papillary thyroid carcinoma (PTC) tissues show that, by measuring different groups of Mueller matrix elements, we can extract the orientation axis parameters. Because many pathological changes affect the well-aligned structures for tissues, the parameters can be used as potential tools in clinical applications for diagnosis purposes. Moreover, using the angle axis information we can separate the

*Address all correspondence to: Hui Ma, E-mail: mahui@tsinghua.edu.cn

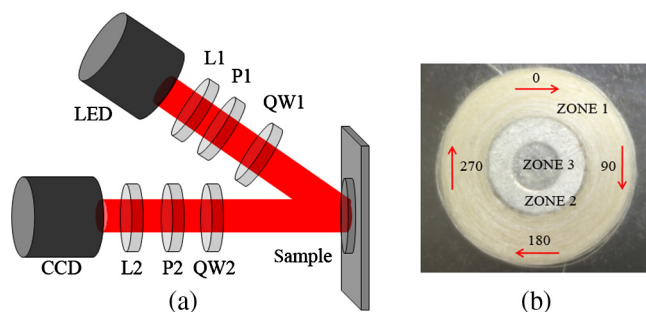


Fig. 1 (a) Schematic of the backscattering Mueller matrix experimental setup. L, lens; P, polarizer; and QW, quarter-wave plate. The polarized light illuminates the sample at about 20 deg to the normal to minimize the surface reflection effects. The diameter of the illumination area from the light-emitting diode is about 1.8 cm, (b) schematic of the silk sample: zone 1 corresponds to the concentric well-aligned silk fibers. The outer diameter of zone 1 is 1 cm; its thickness is 0.5 cm; and the scattering coefficient is 70 cm^{-1} . The diameter of the silk fiber is taken as $1.5 \mu\text{m}$. Zone 2 is a metal spacer with a hole at the center. To ensure a flat imaging surface, a piece of glass plate is placed onto the sample.

orientation influence of samples from the polarization measurements including Mueller matrix imaging. Thus the orientation-independent Mueller matrix elements can reflect the intrinsic microstructural characteristic features of tissue samples.

2 Methods and Materials

2.1 Experimental Setup

The experimental setup and the well-aligned silk sample are shown in Figs. 1(a) and 1(b). In this paper, we use a typical backscattering configuration for Mueller matrix measurements.¹⁵ The polarized light source consists of a light-emitting diode (1 W, center wavelength 630 nm, $\Delta\lambda = 10 \text{ nm}$) and a set of linear polarizer (P1, extinction ratio 500:1, Daheng Optics, Beijing, China) and quarter-wave plate (QW1, Daheng Optics), which control the polarization states of the beam. The incident light illuminates the sample at a 20 deg oblique angle. Backscattered photons from the 1.8-cm diameter illuminated area pass through another set of quarter-wave plate (QW2, Daheng Optics) and linear polarizer (P2, extinction ratio 500:1, Daheng Optics), then are recorded by a 12-bit CCD camera. Before experiments, we calibrated the experimental setup using standard samples with known Mueller matrices, such as the polystyrene microspheres suspended in water. Calibrations show that the maximum errors for the absolute values of all the Mueller matrix elements are about 0.01. In this experiment, we choose six polarization states for the incident light, then measure six corresponding polarization components of the backscattered light. The Mueller matrix elements are calculated from the 36 measurements following a procedure as shown in Ref. 15.

2.2 Materials and MC Simulations

In order to reveal the relationship between the Mueller matrix elements and the orientation of fibrous scatterers, we used specifically designed highly anisotropic fibrous samples as shown in Fig. 1(b). The sample consists of concentric well-aligned fibrous silk strands (zone 1), which are wound around the platform (zone 2) of a metal spacer with a hole at the center (zone 3). In our previous studies, we approximated the silk fibers as

cylindrical scatterers using the SCSM.^{18,19} The circularly aligned silk sample helps us to analyze the Mueller matrices for fibrous scatterers along all directions in the X - Y plane in one measurement. For a deeper understanding on the complicated relationship between the Mueller matrix elements and the microstructure of the scattering medium, we also carried out the MC simulations based on the SCSM. The detailed information on the SCSM, the MC simulation program, and parameters can be found in Ref. 18. The parameters are: the diameter of the cylindrical scatterers corresponding to the substructure of the silk fibers is $1.5 \mu\text{m}$, and the fluctuation of fiber orientation follows a Gaussian distribution of 20 deg full width at half maximum (FWHM). The refractive indices for the silk fiber and surrounding media are 1.59 and 1, respectively. For the well-aligned silk layer (zone 1), its thickness and scattering coefficient are 0.5 cm and 70 cm^{-1} , respectively. During the experiments, to ensure a flat imaging surface, we placed a piece of glass plate onto the samples. Comparisons of the Mueller matrices for samples with and without the glass plate proved that the influence of the glass plate to the measurements is within the experimental error.

Considering potential biomedical applications, we also conducted measurements using histological sections of human PTC samples that are provided by Shenzhen Sixth People's (Nanshan) Hospital.²⁰ The fresh PTC cancerous tissue samples were cut into pieces of a few millimeters thick, fixed in formalin, dehydrated, and embedded in paraffin. Then a nonstained $28\text{-}\mu\text{m}$ thick section is prepared with a microtome as the sample for the backscattering Mueller matrix imaging experiments. From the same paraffin block, a $4\text{-}\mu\text{m}$ thick section was also cut, rehydrated, and stained to make a standard histological plate. Figures 2(a) and 2(b) show the photographs of the unstained $28\text{-}\mu\text{m}$ thick paraffin slices of the PTC tissues, the red circles identify the Mueller matrix imaging areas, and the blue rectangles show the approximated microscope imaging areas. Figures 2(c) and 2(d) show the microscope images of the corresponding hematoxylin and eosin (H-E) stained $4\text{-}\mu\text{m}$ thick paraffin slices from the same PTC tissue samples. Using these samples, we are able to compare directly the polarization images with the microscope images of the H-E stained PTC histological sections. Some pathological studies of the PTC tissues reveal that, during the development for the papillary carcinoma cells, it is sometimes accompanied by inflammatory reactions, which can result in fibrosis formations in the surrounding tissues.²⁰ We can observe in Figs. 2(c) and 2(d) that there are fibers around the PTC cancerous cells.

2.3 Calculation of the Orientation Axis of the Fibers

Both experiments and simulations have shown that for a sample containing fibrous scatterers along a particular direction, as we rotate the sample, therefore, change the orientation of cylindrical scatterers, some of the Mueller matrix elements display periodic intensity variations. In both the experiments and MC simulations, it has been concluded that as the direction of the fibrous structures varies from 0 to 360 deg, the m_{22} , m_{23} , m_{32} , and m_{33} elements repeat four times, whereas the m_{12} , m_{13} , m_{21} , and m_{31} repeat only twice. A closer examination of both the experimental and simulated results reveals that, for normal incidences, the m_{12} , m_{21} , m_{13} , m_{31} , m_{22} , m_{33} , m_{23} , and m_{32} can be fitted to trigonometric forms as shown in Eq. (1).¹⁵ There are three independent parameters that can be extracted from Eq. (1): t [t_1 or t_2 shown in Eq. (2)] is related to the amplitude of the

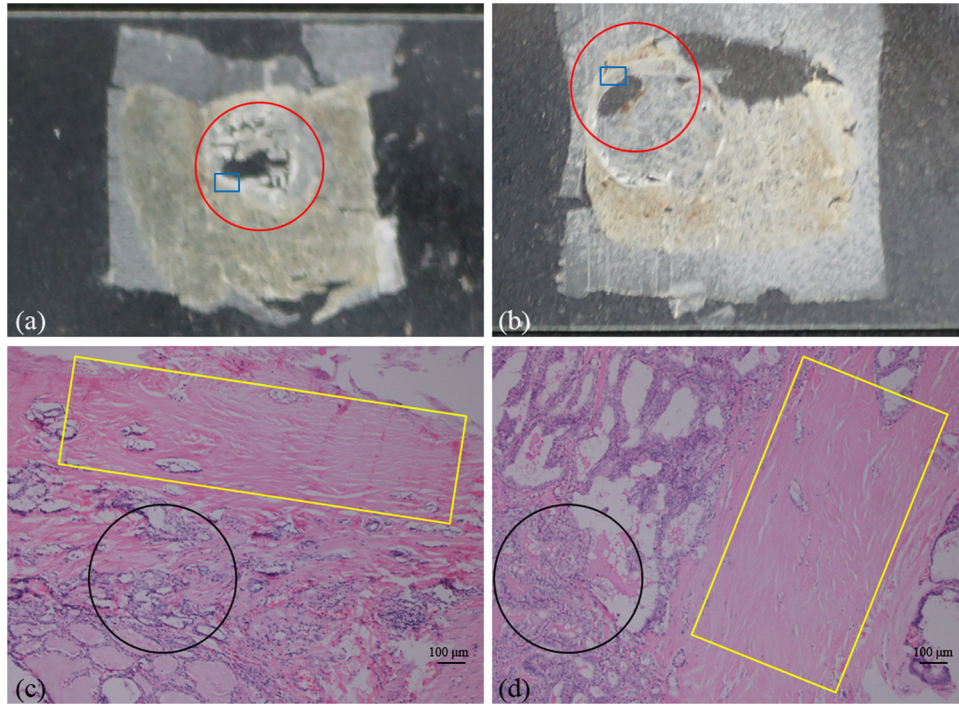


Fig. 2 (a) and (b) The 28- μm thick slices of unstained human papillary thyroid carcinoma (PTC) tissues, the red circles show the Mueller matrix imaging areas (diameter 1 cm), the blue rectangles show the approximated microscope imaging areas in 2(c) and 2(d), (c) and (d) microscope images of the corresponding H-E stained PTC tissues (1.7 mm \times 1.3 mm). The yellow rectangles show the fibers surrounding the PTC cancerous cells, which are indicated by the black circles.

trigonometric curves or the magnitude of anisotropy for the samples, b [shown in Eq. (3)] is related to an offset that can be affected by both the structure and density of the scatterers, and x represents the direction of the fibrous structure. There are two ways to obtain x from the Mueller matrix using either Eqs. (4) or (5). However, x extracted from Eqs. (4) or (5) has four or two periods in a π range, and therefore allows us to determine the alignment angles in a $\pi/4$ range and $\pi/2$ range, respectively. To determine the orientation angle in a π range, we can combine Eq. (5) with a positive or negative value of the m_{13} element (or other Mueller matrix elements) as a determination condition [shown in Eq. (6)]. Therefore, by measuring the m_{12} and m_{13} elements, we can calculate the orientation of the aligned fibrous microstructures

$$\begin{cases} m_{22} = t_1 \cos 4x + b \\ m_{33} = -t_1 \cos 4x + b \\ m_{23} = m_{32} = t_1 \sin 4x \end{cases} \quad \begin{cases} m_{12} = m_{21} = t_2 \cos 2x \\ m_{13} = m_{31} = t_2 \sin 2x \end{cases}, \quad (1)$$

$$\begin{cases} t_1 = \frac{\sqrt{(m_{22}-m_{33})^2 + (m_{23}+m_{32})^2}}{2} \\ t_2 = \sqrt{m_{12}^2 + m_{13}^2} \end{cases}, \quad (2)$$

$$b = \frac{m_{22} + m_{33}}{2}, \quad (3)$$

$$\tan(4x) = \frac{m_{23} + m_{32}}{m_{22} - m_{33}}, \quad (4)$$

$$\tan(2x) = \frac{m_{13}}{m_{12}}, \quad (5)$$

$$x \in \begin{cases} [0, \frac{\pi}{2}] & \text{if } (m_{13} \geq 0) \\ (\frac{\pi}{2}, \pi) & \text{if } (m_{13} < 0) \end{cases}. \quad (6)$$

3 Results and Discussion

Figure 3 shows the experimental backscattering Mueller matrix of the concentrically well-aligned silk fibers. Actually in this paper, we design the silk phantom consisting of fibers wound around a core to show Mueller matrix elements of fibrous scatterers at all angles of orientation instead of rotating the silk fibers from 0 to 360 deg. It can be observed from Fig. 3 that many matrix elements, the m_{12} , m_{13} , m_{31} , m_{21} , m_{22} , m_{33} , m_{23} , and m_{32} , display prominent periodical variations that can be fitted to trigonometric functions of azimuth angle.⁹ It should be pointed out that for anisotropic scattering media with strong birefringence, Mueller matrix elements in the fourth row and fourth column also show periodical intensity changes as the azimuth angle varies. For the cylindrical scattering dominated silk fibers, the anisotropy is mostly represented in the m_{12} , m_{13} , m_{21} , m_{31} , m_{23} , m_{32} , m_{22} , and m_{33} elements. For the media containing strong optical birefringence, however, the anisotropy is mostly represented in the m_{24} , m_{42} , m_{34} , and m_{43} elements.²¹

Figure 4 shows the experimental results of parameter x for the same concentrically aligned silk sample but calculated from different Mueller matrix elements using Eqs. (4) or (5). Figures 4(a) and 4(b) confirm that the parameter x extracted

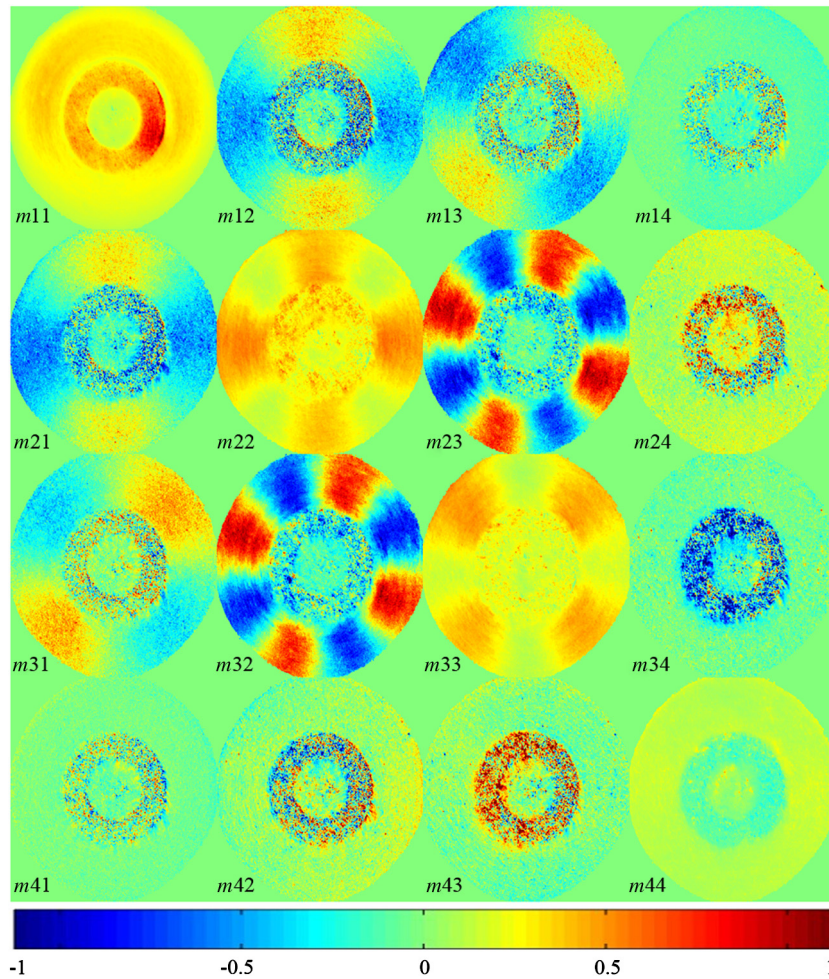


Fig. 3 Experimental results of backscattering Mueller matrix for the concentrically well-aligned silk sample shown in Fig. 1(b). The m_{11} is normalized by its maximum value, and other Mueller matrix elements are normalized by the m_{11} . For better visual effects, the color codes are from -1 to 1 for the m_{11} , m_{22} , m_{33} , and m_{44} , from -0.5 to 0.5 for the m_{23} and m_{32} , and from -0.1 to 0.1 for other elements. As the azimuth angle of the silk fibers varies from 0 to π , the elements show prominent periodical intensity variations.

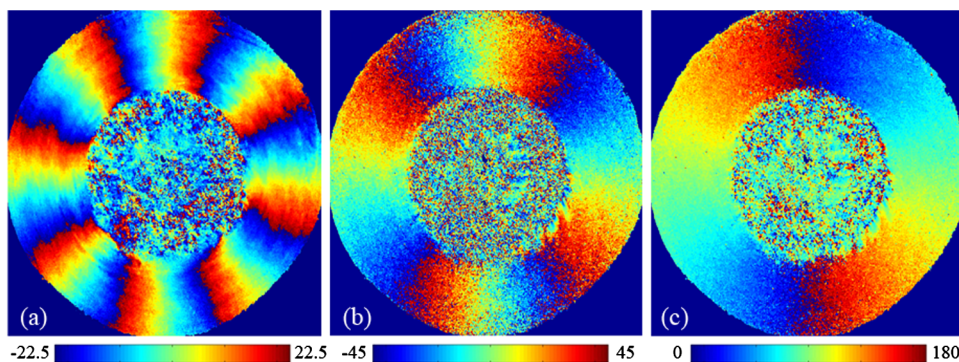


Fig. 4 Experimental results of the parameter x for concentrically aligned silk sample shown in Fig. 1(b): (a) parameter x extracted from Eq. (4), the color code is from -22.5 to 22.5 deg; (b) parameter x extracted from Eq. (5), the color code is from -45 to 45 deg; (c) considering a positive or negative value for the m_{13} element as a determination condition, the parameter x can be expanded to a full π range by using Eqs. (5) and (6), the color code is from 0 to 180 deg.

from Eqs. (4) and (5) has eight and four periods in a 2π range, respectively. For instance, in Fig. 4(a), the silk fibers distributed along $\theta + n\pi/4$ directions cannot be distinguished, whereas in Fig. 4(b), the silk fibers distributed along $\theta + n\pi/2$ directions show the same color codes. As mentioned above, to distinguish the fibrous structures in a full π range, we consider the sign of the m_{13} element as a determination condition. The experimental result shown in Fig. 4(c) is calculated using Eqs. (5) and (6). We can conclude that the parameter x determined by Eqs. (5) and (6) represents the orientation angle of the aligned fiber in the X - Y plane. The experimental results also testify that we can extract an orientation angle information from different groups of Mueller matrix elements. The m_{22} , m_{23} , m_{32} , and m_{33} elements have larger amplitude values compared with other elements and can be measured more precisely. The orientation angles determined by these elements have better immunity to noises. We may use different groups of Mueller matrix elements for different purposes. For instance, in order to extract more accurate information, we may first use the noisy m_{12} , m_{13} , m_{21} , and m_{31} elements for coarse estimations of the fiber orientation in full range, then use the m_{22} , m_{23} , m_{32} , and m_{33} elements, which have smaller periods but better signal-to-noise

ratio, to refine the coarse estimations of the fiber orientation more accurately.

For more detailed examinations of the relationships between parameter x and the orientation distributions of the aligned fibers, we conduct MC simulations based on the SCSM using parameters listed in Sec. 2.3. In the simulations, the directions of the cylindrical scatterers fluctuate around an orientation angle in three-dimensional space following a Gaussian distribution of 20 deg FWHM, and the orientation angle takes different values between 0 and 360 deg in the X - Y plane. The experimental data are the average values calculated for all the silk fibers in zone 1. Figure 5 shows the comparisons between MC simulated (red dashed lines for normal incidence and black circles for 20 deg oblique incidence) and experimental (blue solid lines) results for the silk fibers along the different azimuth directions. As shown in Fig. 5(a), Eq. (5) can only be used to discriminate fibers in a $\pi/2$ range. Figure 5(b) shows that combined with Eq. (6), the m_{12} and m_{13} elements can be used to distinguish fibers in a full π range. The results show clearly that the MC simulations regenerate the dominant features of the experiments, but there are consistent discrepancies between experimental measurement (blue lines) and the MC simulated results at a normal incidence (red

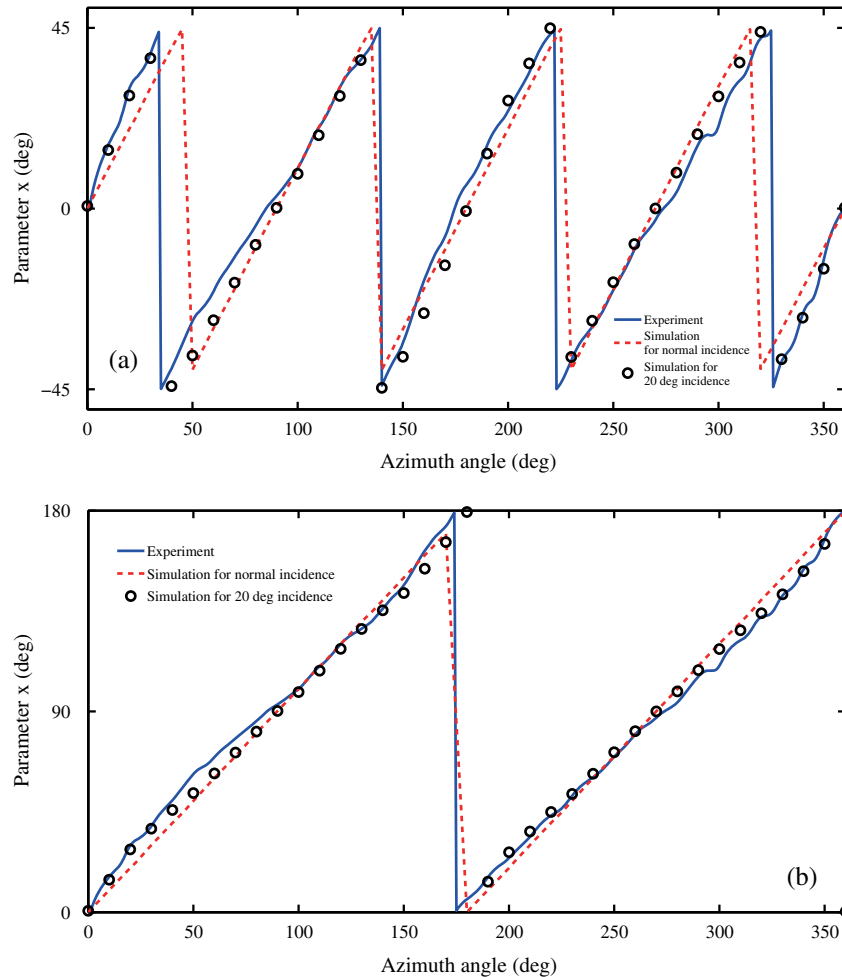


Fig. 5 Comparisons between Monte Carlo (MC) simulated (red dashed lines for normal incidence, black circles for 20 deg oblique incidence) and experimental (blue solid lines) results of the parameter x for cylindrical scatterers along different directions. (a) The angles are calculated by Eq. (5); (b) the angles are calculated by Eqs. (5) and (6). The MC simulations regenerate the dominant features of the experiments. It should be noticed that the oblique incidences of illumination have influence on the values of parameter x .

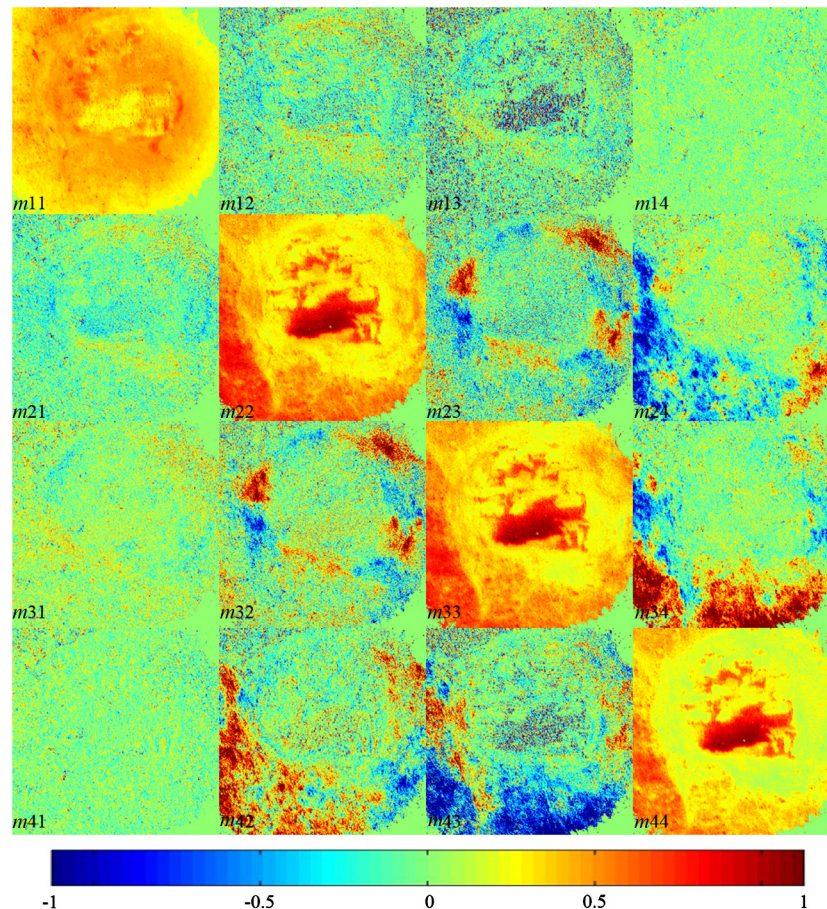


Fig. 6 Experimental results of backscattering Mueller matrix for the unstained PTC sample shown as the red circle area in Fig. 2(a). The m_{11} is normalized by its maximum value, and other Mueller matrix elements are normalized by the m_{11} . The color codes are from -1 to 1 for the m_{11} , m_{22} , m_{33} , and m_{44} , and from -0.1 to 0.1 for other elements.

lines). More simulations corresponding to different incident angles of the illumination beam reveal that this discrepancy comes from the 20 deg oblique incidence of the current experimental setup (shown as black circles).

Biological tissues contain rich fibrous microstructures, such as the collagen and elastin fibers. Many pathological processes are associated with the changes of the aligned fibrous microstructures. Mapping the orientation angles can provide structural information for biomedical diagnosis purposes. In order to verify the potential applications of the parameter x , we measured the backscattering Mueller matrices of human PTC tissues as shown in Fig. 6. The imaging sample is a 28- μm thick slice of unstained cancerous tissue, which shows no distinctive features when examined using both transmission and reflection microscopes. Pathological diagnosis using the corresponding 4 μm H-E stained slice confirmed that the samples are human PTC tissues, and the imaging areas are marked as the red circles in Figs. 2(a) and 2(b). Pathological studies of the H-E stained slices also reveal that, during the early stage of development, the PTC cells sometimes are accompanied by inflammatory reactions and result in fibrosis formations in the surrounding tissues.²⁰ These fibrosis tissues often display well-ordered alignments as shown in Figs. 2(c) and 2(d), and thus larger anisotropy degree compared with the normal thyroid tissues. Figures 7(a) and 7(b) show the parameter x imaging results calculated from Eqs. (4) and (5) for the PTC sample as shown in Fig. 2(a).

Figure 7(c) is the result expanded to a full π range by using Eq. (6). In Fig. 7, the direction changes of fibrosis can be observed clearly. The changes of the parameter x show that the fibrosis structures surrounding the cancerous cells to form a circular area. Figures 8(a) and 8(b) show the parameter x imaging results for the PTC sample as shown in Fig. 2(b) calculated from Eqs. (4) and (5), respectively. Figure 8(c) is the result expanded to a full π range by using Eq. (6). The pathological microscope image shown in Fig. 2(d) confirms the fibers existing in this sample. It can be observed from Figs. 7 and 8 that the parameter x can be used as a clear indicator for these cancer-related fibers. Moreover, the results shown in Figs. 7(a) and 8(a) also confirm that although with a higher degeneracy the parameter x determined by the m_{22} , m_{23} , m_{32} , and m_{33} elements can be measured more precisely. Recent studies have testified that, besides the PTC tissues, some other human cancerous tissues such as the cervical carcinoma in different stages also show characteristic structural changes in the fibrous alignments. Preliminary studies on biological tissues have shown that the parameters proposed in this paper can also be applied to intact tissue specimen. The orientation-related parameter x extracted from the Mueller matrix elements therefore have potential ability for biomedical purposes including cancer detections. Moreover, the MMT method can be combined with the polarized-light microscope to provide more microstructural information of tissue samples, such as the depolarization, birefringence, and densities of small scatterers.

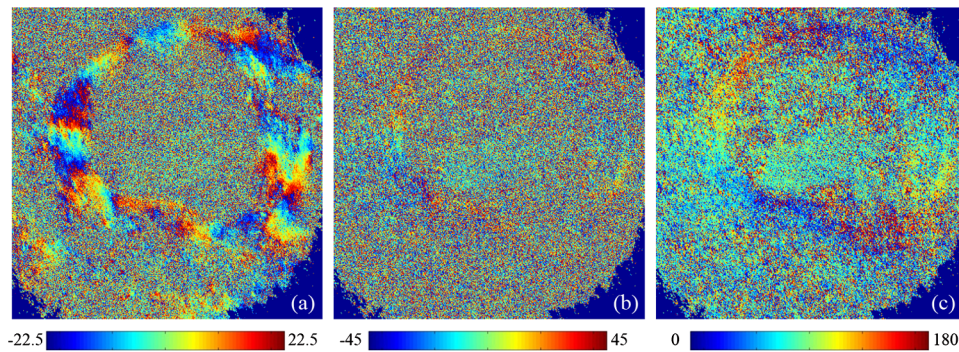


Fig. 7 Experimental results of the parameter x for the unstained PTC sample shown as the red circle area in Fig. 2(a), the diameter of the imaging area is about 1 cm: (a) parameter x extracted from Eq. (4), the color code is from -22.5 to 22.5 deg; (b) parameter x extracted from Eq. (5), the color code is from -45 to 45 deg; (c) considering a positive or negative value for the m_{13} element as a determination condition, the parameter x can be expanded to a full π range by using Eqs. (5) and (6), the color code is from 0 to 180 deg.

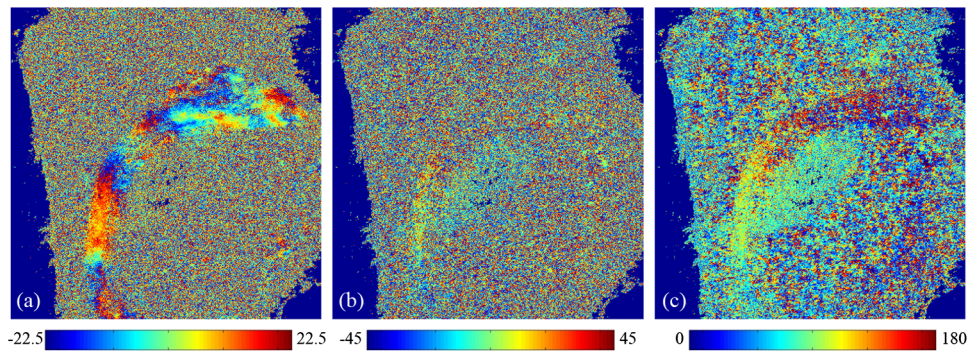


Fig. 8 Experimental results of the parameter x for the unstained PTC sample shown as the red circle area in Fig. 2(b), the diameter of the imaging area is about 1 cm: (a) parameter x extracted from Eq. (4), the color code is from -22.5 to 22.5 deg; (b) parameter x extracted from Eq. (5), the color code is from -45 to 45 deg; (c) considering a positive or negative value for the m_{13} element as a determination condition, the parameter x can be expanded to a full π range by using Eqs. (5) and (6), the color code is from 0 to 180 deg.

The Mueller matrix microscope can be used as a powerful tool for quantitative biomedical diagnosis.

4 Conclusion

Angular distributions are important information for biomedical studies. In this paper, we propose a quantitative analysis technique based on backscattering Mueller matrix for mapping the local orientation axis of aligned fibrous scatterers. By conducting both the experiments on concentrically well-aligned silk fibers and MC simulation based on the SCSM, we extract orientation parameters from different groups of the backscattering Mueller matrix elements including the m_{12} , m_{13} , m_{22} , m_{23} , m_{32} , and m_{33} . We find that among all the 16 Mueller matrix elements, the m_{12} and m_{13} can be used to uniquely determine the orientation axis in a full π range. The m_{22} , m_{23} , m_{32} , and m_{33} elements can only determine the axis of fiber orientation in a narrower range. However, the m_{22} , m_{23} , m_{32} , and m_{33} elements can be measured more precisely, and the angles determined by these elements have better immunity to noises. Moreover, we testify the possible applications of these parameters for human cancerous tissues. The experimental results of unstained human PTC tissues testify that, by measuring the m_{12} and m_{13} elements, we can show the alignment

directions of fibrous microstructures. We also find that one may use the m_{12} , m_{13} , m_{21} , and m_{31} elements for coarse estimations of the fiber orientation, then use the m_{22} , m_{23} , m_{32} , and m_{33} , which have smaller periods and better signal-to-noise ratio, for more accurate measurements. Because many pathological changes affect the well-aligned fibrous structures of tissues, mapping the local orientation of the fibrous tissues can serve as a potential tool for clinical diagnosis purposes. Both the experimental and MC simulated results show the possibilities to separate the influence of orientation and oblique incidences from the Mueller matrices. Thus the orientation-independent Mueller matrix elements can reflect the intrinsic microstructural characteristic features of tissues. Combining with other MMT parameters, we can distinguish the characteristic features of fibers in abnormal and healthy tissues.

Acknowledgments

This work has been supported by the National Natural Science Foundation of China Grants Nos. 11174178, 11374179, and 61205199 and the Knowledge Innovation Program of Basic Research Projects of Shenzhen Grant No. JCY20130402145002404.

References

1. N. Ghosh and I. A. Vitkin, "Tissue polarimetry: concepts, challenges, applications, and outlook," *J. Biomed. Opt.* **16**(11), 110801 (2011).
2. S. L. Jacques, J. C. Ramella-Roman, and K. Lee, "Imaging skin pathology with polarized light," *J. Biomed. Opt.* **7**(3), 329–340 (2002).
3. R. R. Anderson, "Polarized light examination and photography of the skin," *Arch. Dermatol.* **127**(7), 1000–1005 (1991).
4. B. D. Cameron, Y. Li, and A. Nezhuvungal, "Determination of optical scattering properties in turbid media using Mueller matrix imaging," *J. Biomed. Opt.* **11**(5), 054031 (2006).
5. N. Ghosh et al., "Mueller matrix decomposition for polarized light assessment of biological tissues," *J. Biophotonics* **2**(3), 145–156 (2009).
6. M. Dubreuil et al., "Mueller matrix polarimetry for improved liver fibrosis diagnosis," *Opt. Lett.* **37**(6), 1061–1063 (2012).
7. P. G. Ellingsen et al., "Quantitative characterization of articular cartilage using Mueller matrix imaging and multiphoton microscopy," *J. Biomed. Opt.* **16**(11), 116002 (2011).
8. T. Novikova et al., "The origins of polarimetric image contrast between healthy and cancerous human colon tissue," *Appl. Phys. Lett.* **102**(24), 241103 (2013).
9. H. He et al., "A possible quantitative Mueller matrix transformation technique for anisotropic scattering media," *Photonics Lasers Med.* **2**(2), 129–137 (2013).
10. A. Pierangelo et al., "Ex-vivo characterization of human colon cancer by Mueller polarimetric imaging," *Opt. Express* **19**(2), 1582–1593 (2011).
11. A. Pierangelo et al., "Ex vivo photometric and polarimetric multilayer characterization of human healthy colon by multispectral Mueller imaging," *J. Biomed. Opt.* **17**(6), 066009 (2012).
12. A. Pierangelo et al., "Multispectral Mueller polarimetric imaging detecting residual cancer and cancer regression after neoadjuvant treatment for colorectal carcinomas," *J. Biomed. Opt.* **18**(4), 046014 (2013).
13. D. Li et al., "Influence of absorption in linear polarization imaging of melanoma tissues," *J. Innovative Opt. Health Sci.* **7**(3), 1450009 (2014).
14. H. He et al., "Application of sphere-cylinder scattering model to skeletal muscle," *Opt. Express* **18**(14), 15104–15112 (2010).
15. H. He et al., "Two-dimensional and surface backscattering Mueller matrices of anisotropic sphere-cylinder scattering media: a quantitative study of influence from fibrous scatterers," *J. Biomed. Opt.* **18**(4), 046001 (2013).
16. A. Pierangelo et al., "Polarimetric imaging of uterine cervix: a case study," *Opt. Express* **21**(12), 14120–14130 (2013).
17. M. Sun et al., "Probing microstructural information of anisotropic scattering media using rotation independent polarization parameters," *Appl. Opt.* **53**(14), 2949–2955 (2014).
18. T. Yun et al., "Monte Carlo simulation of polarized photon scattering in anisotropic media," *Opt. Express* **17**(19), 16590–16602 (2009).
19. E. Du et al., "Two-dimensional backscattering Mueller matrix of sphere-cylinder birefringence media," *J. Biomed. Opt.* **17**(12), 126016 (2012).
20. E. Du et al., "Mueller matrix polarimetry for differentiating characteristic features of cancerous tissues," *J. Biomed. Opt.* **19**(7), 076013 (2014).
21. J. Chang et al., "Removing the polarization artifacts in Mueller matrix images recorded with a birefringent gradient-index lens," *J. Biomed. Opt.* **19**(9), 095001 (2014).

Biographies of the authors are not available.